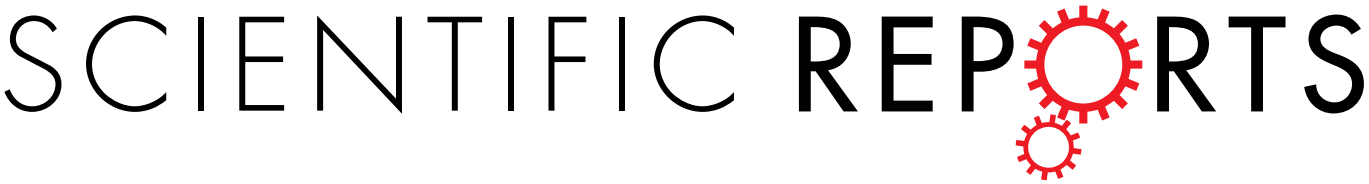

OPEN

Giant Anisotropic Magnetocaloric Effect in Double-perovskite Gd_2CoMnO_6 Single Crystals

Received: 23 August 2017
Accepted: 13 November 2017
Published online: 23 November 2017

J. Y. Moon, M. K. Kim, Y. J. Choi & N. Lee

The magnetocaloric effect (MCE) is described by the change in temperature of a material by magnetic field variation and is a crucial subject in magnetism; it is motivated by the desire to enhance energy-efficient magnetic refrigeration for clean technology. Despite the recent discovery of the giant cryogenic MCE in double perovskites, the role of magnetic anisotropy has not yet been clearly discussed, because of the averaging effect of polycrystalline samples. Here, we investigated the anisotropic MCE in the single-crystal double perovskite Gd_2CoMnO_6. In addition to the ferromagnetic order of the Co^{2+} and Mn^{4+} moments, the large Gd^{3+} moments align below $T_{Gd} = 21$ K, exhibiting an isotropic nature. Because of the intricate temperature development of magnetically hysteretic behaviour and metamagnetism, the change in magnetic entropy along the *c*-axis appears to be relatively small. On the contrary, the smaller but almost reversible magnetization perpendicular to the *c*-axis leads to a large MCE with a maximum entropy change of 25.4 J/kg·K. The anisotropic MCE generates a giant rotational MCE, estimated as 16.6 J/kg·K. Our results demonstrate the importance of magnetic anisotropy for understanding the MCE and reveal essential clues for exploring suitable magnetic refrigerant compounds aiming at magnetic functional applications.

Magnetic materials exhibiting the giant magnetocaloric effect (MCE) have been widely investigated[1–3], and it would be advantageous to replace conventional refrigeration based on vapor compression and realize energy-efficient magnetic refrigeration for clean technology. It is desirable to design and discover new compounds that exhibit the giant MCE for more feasible applications. The giant and/or reversible MCE near room temperature has recently been found in several alloy systems such as $Gd_5(Si_xGe_{1-x})^4$, $MnFeP_{0.45}As_{0.55}$[5] (magnetic entropy change $\Delta S_M = 18.0$ J/kg·K for $\Delta H = 0$–5 T), Ni–Mn–In[6,7] (adiabatic temperature change $\Delta T_{ad} = 6.2$ K for $\Delta H = 0$–1.9 T), and $La(Fe,Si)_{13}$[8] ($\Delta S_M = 16$ kJ/m^3·K for $\Delta H = 0$–2 T), which offer potential refrigeration techniques for domestic usage and microelectronic devices. Cryogenic magnetic refrigeration is also essential for obtaining sub-Kelvin temperatures as a substitute for ^{3}He/^{4}He dilution refrigeration, whose cost continues to increase, and for hydrogen gas liquefaction, which is utilized as an alternative fuel. The MCE has been explored in many insulating oxides[9–13], which can be easily manufactured on account of the chemical stability along with the avoidance of the refrigeration inefficiency driven by eddy current losses. Recently, the giant cryogenic MCE was discovered in several transition metal oxides such as Dy_2CoMnO_6[10] ($\Delta S_M = 9.3$ J/kg·K for $\Delta H = 0$–7 T), $HoMnO_3$[11] ($\Delta S_M = 13.1$ J/kg·K for $\Delta H = 0$–7 T)., $GdCrO_4$[12] ($\Delta S_M = 29.0$ J/kg·K for $\Delta H = 0$–9 T), and $HoCrO_4$[13] ($\Delta S_M = 31.0$ J/kg·K for $\Delta H = 0$–8 T). However, most of the studies were performed on polycrystalline forms, preventing detailed characterization of the intrinsic properties of the giant MCE associated with magnetic and crystalline anisotropy.

To investigate the influence of the anisotropic characteristics on the giant MCE in one of the transition metal oxides, we have synthesized single crystals of the double perovskite Gd_2CoMnO_6 (GCMO) using the conventional flux method[14]. Double perovskite R_2CoMnO_6 (R = La, …, Lu) compounds, where Co^{2+} and Mn^{4+} ions are alternately located in corner-shared octahedral environments, exhibit assorted physical properties such as metamagnetism[15–17], exchange bias[18,19], the re-entrant spin-glass state[20,21], and multiferroicity[16,22–24] because of the intricate magnetic interactions and ionic valence/antisite disorders between mixed-valence magnetic ions. The ferromagnetic order originates from the dominant Co^{2+} and Mn^{4+} superexchange interactions, and its transition temperature varies linearly from 204 K for La_2CoMnO_6[25] to 48 K for Lu_2CoMnO_6[26] as the size of the rare earth ions decreases. GCMO crystallizes in a monoclinic $P2_1/n$ double-perovskite structure with a unit cell of

Department of Physics and IPAP, Yonsei University, Seoul, 120-749, Korea. Correspondence and requests for materials should be addressed to Y.J.C. (email: phylove@yonsei.ac.kr) or N.L. (email: eland@yonsei.ac.kr)

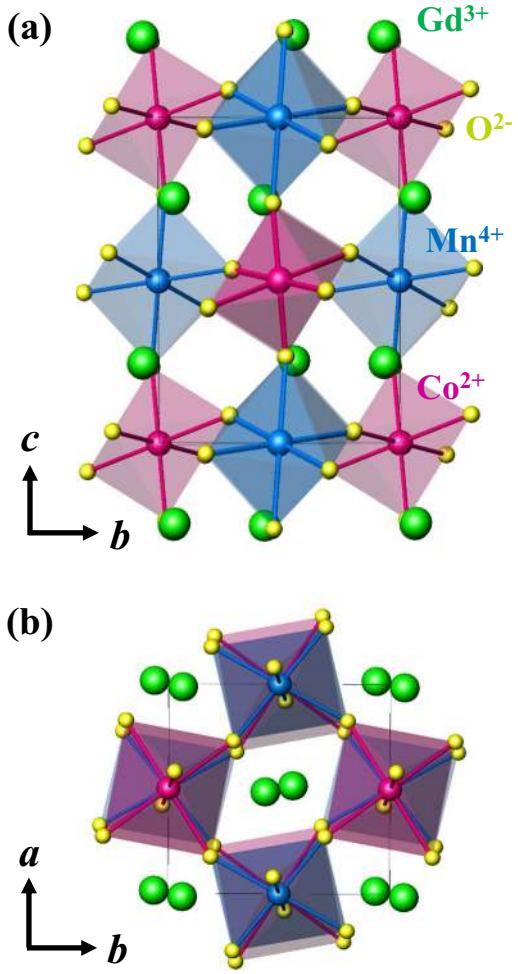

Figure 1. Crystallographic structure of a GCMO crystal. (**a**,**b**) Views of the crystal structure of double perovskite GCMO crystal from the *a*- and *c*-axes, respectively. The green, pink, blue, and yellow spheres represent Gd^{3+}, Co^{2+}, Mn^{4+}, and O^{2-} ions, respectively.

$a = 5.3158$ Å, $b = 5.6050$ Å, $c = 7.5759$ Å, and $\beta = 89.9541°$. The crystal structures viewed from the *a*- and *c*-axes are depicted in Fig. 1(a) and (b), respectively. The oxygen octahedral cages are considerably distorted due to the comparatively small radius of the Gd^{3+} ion. In a previous study, the polycrystalline form of GCMO revealed a large maximum entropy change of $\Delta S_M \approx 24$ J/kg·K[27], attributed to the large magnetic moments of Gd^{3+} ions.

From our examination of the anisotropic MCE in GCMO single crystals, we only found a ΔS_M value of half that in the polycrystalline specimen along the magnetic easy *c*-axis despite the large magnetization (*M*) at an applied magnetic field (*H*). The significant reduction in MCE was caused by the strong temperature (*T*) dependence of the magnetic hysteresis and metamagnetic transition. Instead, the isothermal *M* perpendicular to the *c*-axis exhibited almost reversible hysteretic behaviour, which contributed to the giant MCE associated with the magnetic entropy change $\Delta S_M = 25.4$ J/kg·K and adiabatic temperature change $\Delta T_{ad} = 7.3$ K in $\Delta H = 0$–9 T. As a result, the highly-anisotropic ΔS_M produced a giant rotational MCE, estimated as 16.6 J/kg·K at 4 K. These results clearly suggest that a meticulous understanding of strongly anisotropic characteristics is crucial for finding improved functional properties in double-perovskite compounds.

Results and Discussion

The anisotropic magnetic properties of GCMO single crystals were examined parallel ($H//c$) and perpendicular to the *c*-axis ($H \perp c$). The *T* dependence of the magnetic susceptibility, $\chi = M/H$, was measured upon warming at $\mu_0 H = 0.2$ T after zero-*H*-cooling (ZFC χ) and upon cooling at the same field (FC χ), as shown in Fig. 2(a) and (b), respectively. As *T* decreases, χ increases smoothly until exhibiting a sharp rise at $T_C = 112$ K, ascribed to the ferromagnetic order of the Co^{2+} ($S = 3/2$) and Mn^{4+} ($S = 3/2$) moments. The ferromagnetic behaviour was characterized by the positive Curie *T* determined by the Curie-Weiss law. T_C was determined by the *T* derivative of χ and by the sharp anomaly in the *T* dependence curve of the heat capacity divided by the temperature (C/T) at zero magnetic field (Fig. 2(c)). Reducing T_C further, FC χ reaches an approximate plateau. In contrast, ZFC χ decreases at the beginning of the warming from 2 K and the slope of χ changes at around $T_{Gd} = 21$ K, below which C/T exhibits an abrupt increase, indicating the ordering of the Gd^{3+} moments. Above T_{Gd}, the χ increases gradually due to the thermally activated domain wall motions. Just below T_C, the ZFC χ shows a distinct peak, which

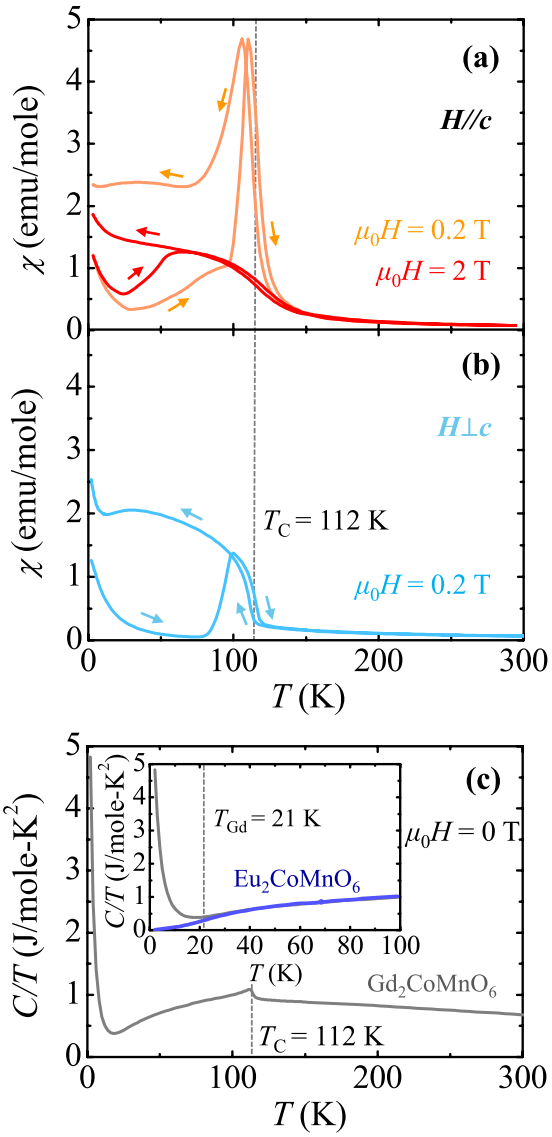

Figure 2. Characterization of temperature-dependent physical properties in a GCMO crystal. (**a**,**b**) Temperature dependence of the magnetic susceptibility, $\chi = M/H$, of double perovskite GCMO single crystal parallel ($H//c$, $\mu_0 H = 0.2$ T and 2 T) and perpendicular ($H \perp c$, $\mu_0 H = 0.2$ T) to the c-axis, respectively, measured upon warming from 2 to 300 K after zero-field-cooling and upon cooling at the same field. The vertical dashed line indicates the ferromagnetic transition temperature, $T_C = 112$ K. (**c**) Temperature dependence of specific heat divided by temperature, C/T, measured at zero magnetic field. The inset shows a comparison of C/T up to 100 K between GCMO and Eu_2CoMnO_6 measured at zero magnetic field. The vertical dashed line denotes the ordering temperature of Gd^{3+} moments as $T_{Gd} = 21$ K.

signifies an additional domain wall de-pinning process. At $\mu_0 H = 2$ T, ZFC and FC χ's exhibit conventional ferromagnetic behaviour without any sharp anomaly near T_C. The T at which the ZFC χ and FC χ curves start to split is observed, indicating the onset of magnetic irreversibility. The thermally hysteretic behaviour of the χ around T_C indicates the first-order nature of the transition. The χ for the two different orientations at $\mu_0 H = 0.2$ T exhibiting a strong magnetic anisotropy near T_C indicates that the Co^{2+} and Mn^{4+} spins are mainly aligned along the c-axis.

To estimate the entropy change based solely on the spin order of Gd^{3+} ions, ΔS_{Gd}, the C/T for Eu_2CoMnO_6, which includes nonmagnetic Eu^{3+} ions with a similar ionic radius to Gd^{3+} ions, was measured, as shown in the inset of Fig. 2(c). The ΔS_{Gd} below T_{Gd} was obtained by integrating C/T by T (2–21 K) for GCMO after subtracting the data from Eu_2CoMnO_6. The calculated ΔS_{Gd} was 17.3 J/mole·K, which is 50% of the expected value of the fully saturated Gd^{3+} moments, i.e., $2R \ln(2J+1) = 34.6$ J/mole·K, where R is the gas constant and J is the total angular momentum ($J = 7/2$ for the Gd^{3+} ion).

Figure 3(a) and (b) display the isothermal M for the two different orientations, measured up to $\mu_0 H = 9$ T at 2 K. The initial M curve at $H//c$ exhibits a gradual increase as H increases before a sudden jump at 6.2 T. The M at the maximum H of 9 T is found to be 15.7 μ_B/f.u., which is 72% of the completely saturated moments by considering the effective magnetic moment of a Gd^{3+} ion as $\mu_{Gd} = 7.98$ μ_B. The consecutive sweeping of H between

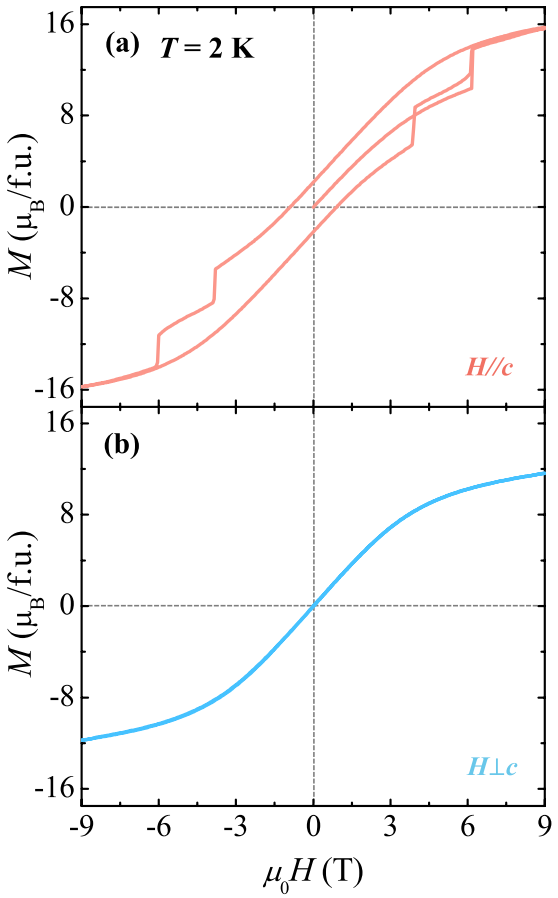

Figure 3. Anisotropic isothermal magnetization of a GCMO crystal at 2 K. (**a**) Full magnetic hysteresis curve of isothermal magnetization along the *c*-axis measured at 2 K up to $H = 9$ T. (**b**) Magnetic field dependence of magnetization perpendicular to the *c*-axis measured at 2 K up to $H = 9$ T.

+9 and −9 T leads to the sharp double-step metamagnetic transitions at $H = \pm 3.9$ and ± 6.2 T. Consequently, the full curve exhibits narrow hysteretic behaviour with the remanent M as $M_r = 2.1$ μ_B/f.u. and the coercive field as $H_c = 0.9$ T. In contrast, the M at $H \perp c$ varies smoothly without any magnetic hysteresis. Regardless of the hard magnetic axis for the ferromagnetic Co^{2+} and Mn^{4+} sublattice, the large magnetic moment of 11.6 μ_B/f.u. at 9 T implies the somewhat isotropic nature of the Gd^{3+} spins associated with the half-filled 4*f* electronic configuration. In other words, the difference of the M values at 9 T between the two orientations is caused by the Co^{2+} and Mn^{4+} spins mainly aligned along the *c*-axis.

The plausible cause for the features of the metamagnetic transitions[18,28] found in the fully hysteretic M curve at $H//c$ (Fig. 3(a)) can be determined from the distinctive magnetic anisotropy between Gd^{3+} and Co^{2+}/Mn^{4+} moments. After ZFC, the Co^{2+} and Mn^{4+} moments are mostly in a parallel or antiparallel arrangement along the *c*-axis, while the Gd^{3+} moments are oriented in random directions reflecting the isotropic character. Upon increasing H, the continuous increase of M up to 10.4 μ_B/f.u. is mainly caused by the alignment of Gd^{3+} moments along with the flipping of only the partial Co^{2+} and Mn^{4+} spins due to the large magnetic anisotropic energy. At 6.2 T, the abrupt jump of M occurs because the Zeeman energy of the Co^{2+}/Mn^{4+} sublattice overcomes the anisotropic energy. The gradual decrease in H from +9 T indicates the reduction of M until it encounters the two consecutive metamagnetic transitions, originating from the flipping of the Gd^{3+} spins and then the Co^{2+} and Mn^{4+} spins, respectively. This assumption is compatible with the magnetically anisotropic energy of the Co^{2+} and Mn^{4+} spins being larger than that of the Gd^{3+} spins. Although the postulation of rather isotropic nature of Gd^{3+} moments gives moderate interpretation for isothermal M at 2 K, the narrow hysteretic behaviour with a small M_r may indicate small degree of interaction between Gd^{3+} and ferromagnetic Co^{2+}/Mn^{4+} sublattices. Upon decreasing H from +9 T, the negative exchange coupling between Gd^{3+} and Co^{2+}/Mn^{4+} spins accompanied by a smaller magnetocrystalline anisotropy energy and larger moment of Gd^{3+} ions leads to the progressive decrease in the net Gd^{3+} moments, followed by the considerable reduction of M_r.

Figure 4 presents the full anisotropic curves of M up to 9 T at various T ($T = 5$, 10, 40, and 100 K). At 5 K and $H//c$, the double-step metamagnetic transitions broaden, while the remanent M and coercive field appear to be enhanced as $M_r = 2.4$ μ_B/f.u. and $H_c = 1.1$ T. At 10 K, the area inside the magnetic hysteresis loop along $H//c$ is considerably reduced with the shift in the metamagnetic transitions to lower H, but M_r and H_c are almost maintained. At $H \perp c$, a very narrow but large magnetic hysteresis loop is observed, presumably because of a weakened

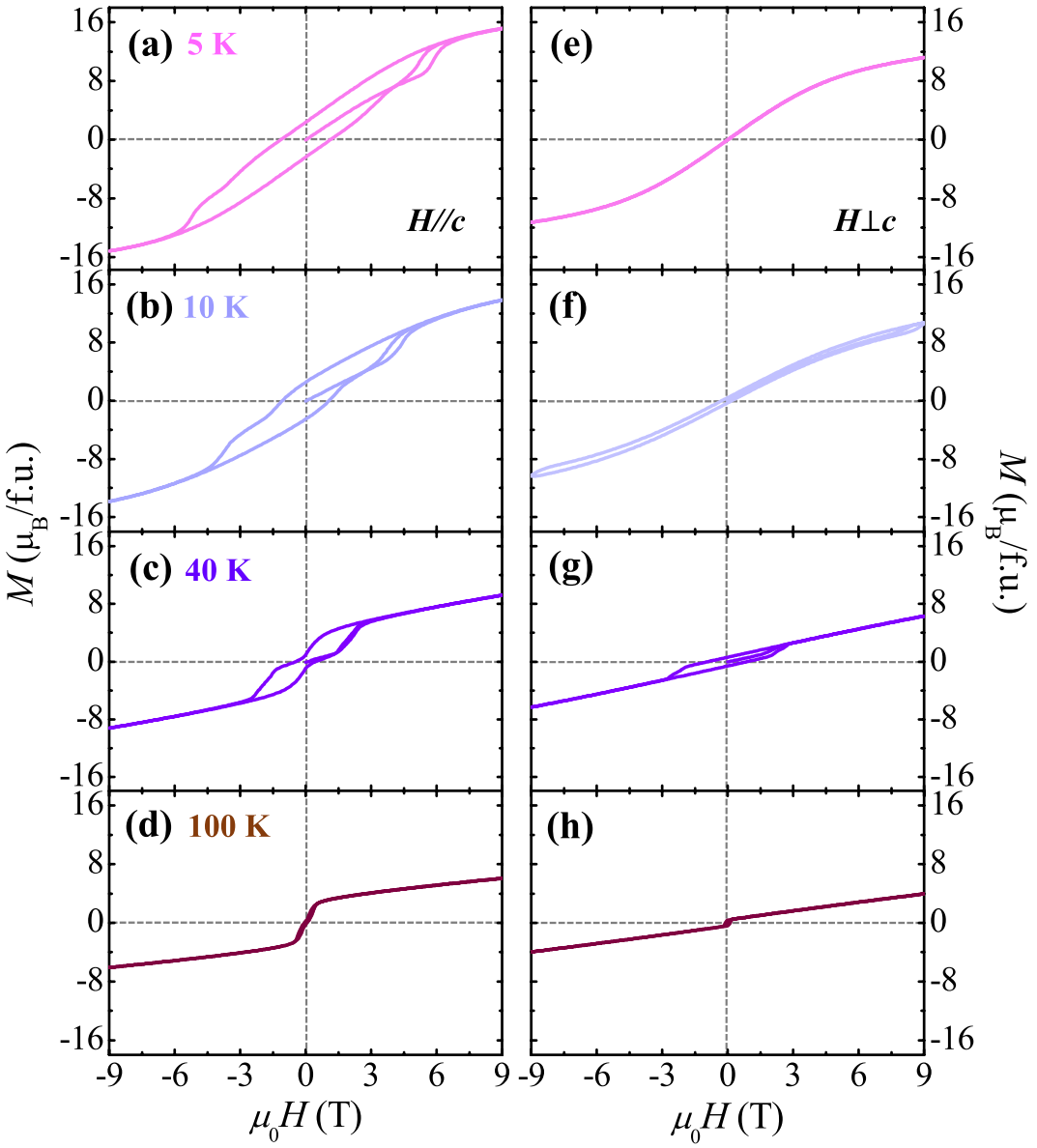

Figure 4. Temperature development of isothermal magnetization. Isothermal magnetizations (**a**–**d**) parallel and (**e**–**h**) perpendicular to the *c*-axis measured at $T = 5$, 10, 40 and 100 K, respectively, up to $H = 9$ T.

magnetic anisotropy due to thermal energy. As T increases further, the area of the magnetic hysteresis loop rapidly shrinks and M_r and H_c also decrease. At 100 K, a slight hysteretic behaviour remains but the metamagnetic transitions almost vanish.

Based on the distinctive magnetic properties for the two different orientations, an anisotropic MCE in the GCMO was obtained by measuring the initial M curves with dense T steps ranging from 2 to 180 K in Fig. 5. In contrast to the typical reduction of M values with the increase in T, the initial M curves at $H//c$ develops in a complicated manner. The sharp steps of the metamagnetic transitions at 2 K move progressively to lower H and become broader as T increases. For this reason, the M value in a given H regime is lower than that at higher T. In the inset of Fig. 5(a), the isothermal M values measured at 5, 10, and 15 K are magnified. The green shaded areas represent specific examples of the reversed order of magnitude for the M values. As T is further increased, the occurrence of the reversed order shifts gradually to the lower H regime. At $H \perp c$, a small but broad transition feature also occurs at some temperature regime while moving to lower H as T is further increased, however, the overall magnitude of M is reduced in most of the regime of H with increasing T, as shown in the inset of Fig. 5(b).

At a given T, the isothermal magnetic entropy change, ΔS_M, can be obtained from the initial M curves using the Maxwell relation:

$$\Delta S_M(T, H) = -\mu_0 \int_0^{H_f} \frac{\partial M(T, H)}{\partial T} dH \quad (1)$$

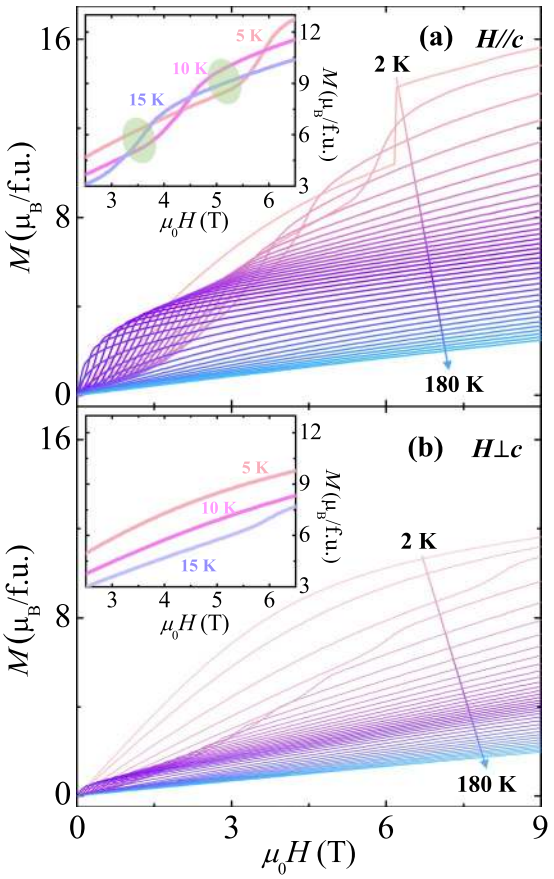

Figure 5. Initial magnetization curves in a wide range of temperatures. (**a**) Initial curves of isothermal magnetization at $H//c$ and various temperatures varying from 2 to 180 K. The inset shows the magnified region of magnetization for $T = 5$, 10, and 15 K. The green shaded ellipses indicate the reversed order of magnetization magnitudes due to the shift in metamagnetic transitions according to T. (**b**) Initial curves of isothermal magnetization at $H \perp c$ and various temperatures varying from 2 to 180 K. The inset shows the magnified region of magnetization for $T = 5$, 10, and 15 K.

where μ_0 is the magnetic permeability in vacuum, H_f is the end point of H for the integral ($H_f = 3$, 5, 7, and 9 T), and the T gradient of M, $\frac{\partial M(T,H)}{\partial T}$, was calculated approximately from the slope of two adjacent data points. The T dependence of the estimated entropy changes, $\Delta S_M(T)$, are plotted in Fig. 6(a) and (b), respectively for $H//c$ and $H \perp c$ with the H regimes of $\Delta H = 0$–3, 0–5, 0–7, and 0–9 T. The ΔS_M values for both orientations exhibit broad peaks at T_C, where the ΔS_M values are found to be 6.2 and 2.7 J/kg·K for $H//c$ and $H \perp c$, respectively. The much larger magnitude of ΔS_M at T_C for $H//c$ describes the magnetic easy c-axis with respect to the ferromagnetic order of Co^{2+} and Mn^{4+} moments. At $H//c$, even with the large M at 2 K, the intercrossed isothermal M values due to the T development of metamagnetic transitions, as depicted in Fig. 5(a), results in a substantial cancellation of ΔS_M. Consequently, a complicated T dependence of ΔS_M is observed below T_{Gd} for $\Delta H = 0$–3 and 0–5 T, and even negative values of ΔS_M are revealed for $T = 20$–90 K. The maximum ΔS_M of 12.1 J/kg·K, found at 8 K for $\Delta H = 0$–9 T, is smaller than the magnitude from the recent observation in the polycrystalline specimen. At $H \perp c$, the near-absence of the estimated loss for ΔS_M generates a large magnitude of ΔS_M, shown as a peak at low T, followed by a steep decrease in ΔS_M. The maximum MCE at 5 K for $\Delta H = 0$–9 T is estimated as $\Delta S_M = 25.4$ J/kg·K.

By taking advantage of the strong magnetic anisotropy due to the distinctive characteristics of the double perovskite GCMO compound, the rotating MCE was measured by the angular dependence of ΔS_M, denoted as ΔS_θ, where θ is the angle deviating from the c-axis, i.e., $\theta = 0°$ for $H//c$ and $\theta = 90°$ for $H \perp c$ (Inset of Fig. 7). Figure 7 shows ΔS_θ obtained at 4 and 8 K for $\Delta H = 0$–9 T. As there is a different T dependence of ΔS_M between $H//c$ and $H \perp c$, the angle-dependent modulation of ΔS_θ varies strongly with T. At 8 K, ΔS_θ negligibly changes with the rotation of θ to 30° and increases linearly above 30°. The maximum ΔS_θ was evaluated as only 7.8 J/kg·K. At 4 K, on the contrary, the continued variation of ΔS_θ by θ rotation generates a giant rotational MCE as the maximum change of 16.6 J/kg·K, which would be beneficial for rotary magnetic refrigerator technology. The maximum difference of ΔS_θ in the GCMO is comparable to the other rotating magnetic refrigerants such as $HoMn_2O_5$[29] (12.4 J/kg·K for $\Delta H = 0$–7 T) and DyNiSi[30] (17.6 J/kg·K for $\Delta H = 0$–5 T).

A more feasible aspect of MCE can be attained as the adiabatic T change, ΔT_{ad}, from the following equation:

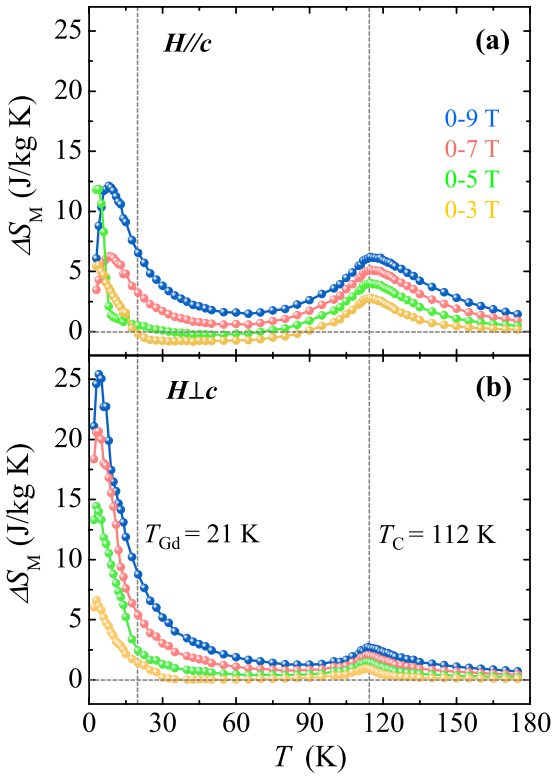

Figure 6. Anisotropic magnetocaloric effect in GCMO. Temperature dependence of magnetic entropy change, ΔS_M, obtained by integrating the temperature gradient of the initial magnetization curves in Fig. 4 for (**a**) $H//c$ and (**b**) $H\perp c$ with magnetic field regimes of $\Delta H = 0$–3 T (yellow), 0–5 T (green), 0–7 T (red), and 0–9 T (blue).

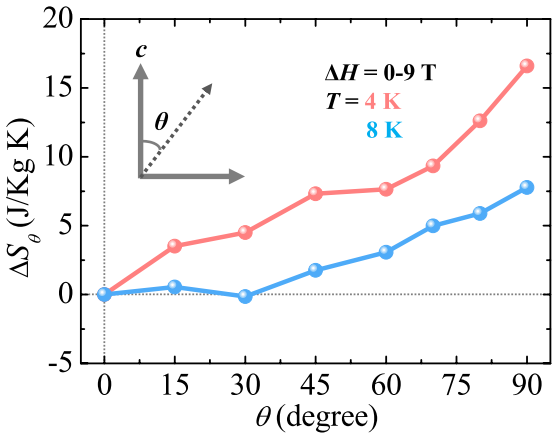

Figure 7. Rotating magnetocaloric effect in GCMO. Angular dependence of magnetic entropy change, ΔS_θ, at $T = 4$ and 8 K with $\Delta H = 0$–9 T. θ is the angle deviating from the c-axis, i.e., $\theta = 0°$ for $H//c$ and 90° for $H \perp c$.

$$\Delta T_{ad}(T) = -\mu_0 \int_0^{H_f} \frac{T}{C(T, H)} \frac{\partial M(T, H)}{\partial T} dH \quad (2)$$

where $C(T, H)$ is the heat capacity at a given T and H. In many cases, C appears to be independent of the applied H, thus, it can be considered as a constant for the integral. However, in GCMO, the T dependence of C/T clearly varies depending on the magnitude of the applied H, as shown in Fig. 8(a) and (b) for $H//c$ and $H \perp c$, respectively, measured at $H = 0$, 3, 5, 7, and 9 T. At $H//c$, the C/T at very low temperatures decreases with H along with the emergence of a broad peak shifting to higher T. As T increases further, C/T decreases more slowly as H gradually increases. Therefore, the order of magnitude of C/T with respect to H is reversed at about 4 K. The C/T for $H \perp c$ exhibits similar T and H dependences as $H//c$. The C/T exhibits a greater reduction as H increases

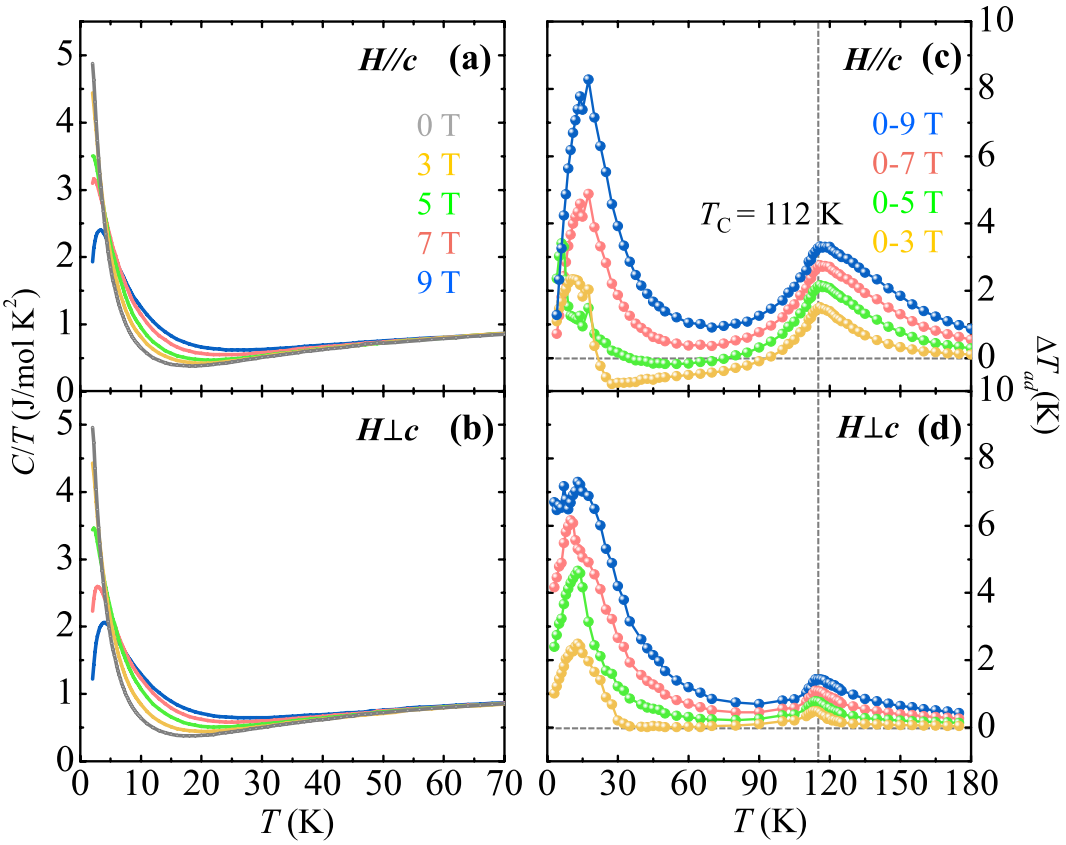

Figure 8. Adiabatic temperature changes in GCMO. (**a**,**b**) Temperature dependence of *C*/*T*, measured at (**a**) *H*//*c* and (**b**) $H \perp c$ with various magnetic fields, $H = 0$, 3, 5, 7, and 9 T, shown at $T = 2$–70 K. (**c**,**d**) Temperature dependence of adiabatic temperature change, ΔT_{ad}, estimated from integrating the temperature gradient of the initial magnetization curves multiplied by the corresponding reciprocal of *C*/*T* for (**c**) *H*//*c* and (**d**) $H \perp c$ with magnetic field regimes of $\Delta H = 0$–3 T (yellow), 0–5 T (green), 0–7 T (red), and 0–9 T (blue).

at the very low *T* regime with a further shift of the peak to higher *T*. ΔS_{Gd} is also estimated from *C*/*T* taken at 9 T for *H*//*c*. $\Delta S_{Gd} = 23.7$ J/mole·K, which is about 69% of the value, assuming full saturation of Gd^{3+} moments, consistent with the measured magnetization at 9 T (Fig. 3(a)). Figure 8(c) and (d) display the *T* dependence of ΔT_{ad}, estimated for *H*//*c* and $H \perp c$, respectively, with $\Delta H = 0$–3, 0–5, 0–7, and 0–9 T. At *H*//*c*, the *T* dependence of ΔT_{ad} behaves similarly to that of ΔS_M. For $\Delta H = 0$–9 T, starting from $\Delta T_{ad} = 1.3$ K at 2 K, ΔT_{ad} increases with *T* and reaches 8.3 K at the peak position as $T = 17.0$ K. However, the estimated *T* dependence of ΔT_{ad} for $H \perp c$ was strongly influenced by the reciprocal of *C*/*T* during the calculation of the integral. Interestingly, the ΔT_{ad} for $\Delta H = 0$–9 T maintains its magnitude between 6.5 and 7.3 K up to $T = 17.0$ K, suggesting that the MCE steadily covers the wide range of the low *T* regime for $H \perp c$.

In summary, we explored the anisotropy of the magnetic and magnetocaloric properties of single-crystal double perovskite GCMO. Contrary to the anticipated large MCE along the magnetic easy *c*-axis, we attained a maximum entropy change of only half the magnitude of that found in the polycrystalline specimen. This substantial reduction is attributed to the intricate temperature evolution of metamagnetic transitions. Alternatively, an almost reversible hysteretic behaviour of isothermal magnetization perpendicular to the *c*-axis results in a large entropy change of $\Delta S_M = 25.4$ J/kg·K, and thus the giant rotational MCE is taken as $\Delta S_\theta = 16.6$ J/kg·K at 4 K. The strongly anisotropic magnetic properties of the double-perovskite compound offer essential clues for the fundamental and applied research on magnetic materials, aiming to enhance the functional properties.

Methods

Rod-shaped single crystals of GCMO were grown using the conventional flux method with Bi_2O_3 flux in air. The stoichiometric ratio of Gd_2O_3, Co_3O_4, and MnO_2 powders was mixed and ground in a mortar, followed by pelletizing and calcining at 1000 °C for 12 h. The calcined pellet was reground and sintered at 1100 °C for 24 h. The same sintering procedure after regrinding was performed at 1200 °C for 48 h. A mixture of pre-sintered polycrystalline powder and Bi_2O_3 flux at a 1:12 ratio was heated to 1300 °C in a Pt crucible. It was melted at the soaking temperature for 5 h, slowly cooled to 985 °C at a rate of 2 °C/h, and cooled to room temperature at a rate of 250 °C/h. The temperature and magnetic field dependences of the DC magnetization, *M*, were examined by a vibrating sample magnetometer at $T = 2$–300 K and $H = -9$-9 T using a Physical Properties Measurement System (PPMS, Quantum Design, Inc.). The temperature dependence of specific heat, *C*, at various magnetic fields was measured with the standard relaxation method using the PPMS.

References

1. Pecharsky, V. K. & Gschneidner, K. A. Jr Magnetocaloric effect and magnetic refrigeration. *Journal of Magnetism and Magnetic Materials* **200**, 44–56, https://doi.org/10.1016/S0304-8853(99)00397-2 (1999).
2. GschneidnerJr, K. A., Pecharsky, V. K. & Tsokol, A. O. Recent developments in magnetocaloric materials. *Reports on Progress in Physics* **68**, 1479 (2005).
3. Yu, B. F., Gao, Q., Zhang, B., Meng, X. Z. & Chen, Z. Review on research of room temperature magnetic refrigeration. *International Journal of Refrigeration* **26**, 622–636, https://doi.org/10.1016/S0140-7007(03)00048-3 (2003).
4. Pecharsky, V. K. & Gschneidner, J. K. A. Giant Magnetocaloric Effect in $Gd_5(Si_2Ge_2)$. *Physical Review Letters* **78**, 4494–4497 (1997).
5. Tegus, O., Bruck, E., Buschow, K. H. J. & de Boer, F. R. Transition-metal-based magnetic refrigerants for room-temperature applications. *Nature* **415**, 150–152 (2002).
6. Manosa, L. *et al*. Giant solid-state barocaloric effect in the Ni-Mn-In magnetic shape-memory alloy. *Nat Mater* **9**, 478–481 (2010).
7. Liu, J., Gottschall, T., Skokov, K. P., Moore, J. D. & Gutfleisch, O. Giant magnetocaloric effect driven by structural transitions. *Nat Mater* **11**, 620–626, http://www.nature.com/nmat/journal/v11/n7/abs/nmat3334.html#supplementary-information (2012).
8. Lyubina, J., Schäfer, R., Martin, N., Schultz, L. & Gutfleisch, O. Novel Design of $La(Fe,Si)_{13}$ Alloys Towards High Magnetic Refrigeration Performance. *Advanced Materials* **22**, 3735–3739, https://doi.org/10.1002/adma.201000177 (2010).
9. Phan, M.-H. & Yu, S.-C. Review of the magnetocaloric effect in manganite materials. *Journal of Magnetism and Magnetic Materials* **308**, 325–340, https://doi.org/10.1016/j.jmmm.2006.07.025 (2007).
10. Ganeshraj, C., Pradheesh, R. & Santhosh, P. N. Structural, magnetic, transport and magnetocaloric properties of metamagnetic $DyMn_{0.5}Co_{0.5}O_3$. *Journal of Applied Physics* **111**, 07A914, https://doi.org/10.1063/1.3672067 (2012).
11. Midya, A. *et al*. Magnetocaloric effect in $HoMnO_3$ crystal. *Applied Physics Letters* **96**, 142514, https://doi.org/10.1063/1.3386541 (2010).
12. Palacios, E. *et al*. Effect of Gd polarization on the large magnetocaloric effect of $GdCrO_4$ in a broad temperature range. *Physical Review B* **93**, 064420 (2016).
13. Midya, A., Khan, N., Bhoi, D. & Mandal, P. 3d-4f spin interaction induced giant magnetocaloric effect in zircon-type $DyCrO_4$ and $HoCrO_4$ compounds. *Applied Physics Letters* **103**, 092402, https://doi.org/10.1063/1.4819768 (2013).
14. Kim, M. K. *et al*. Investigation of the magnetic properties in double perovskite R_2CoMnO_6 single crystals (R = rare earth: La to Lu). *Journal of Physics: Condensed Matter* **27**, 426002 (2015).
15. Blasco, J. *et al*. Evidence of large magneto-dielectric effect coupled to a metamagnetic transition in Yb_2CoMnO_6. *Applied Physics Letters* **107**, 012902, https://doi.org/10.1063/1.4926403 (2015).
16. Wang, L. *et al*. Effect of metamagnetism on multiferroic property in double perovskite Sm_2CoMnO_6. *Journal of Applied Physics* **117**, 17D914, https://doi.org/10.1063/1.4917517 (2015).
17. Su, J. *et al*. Magnetic and dielectric properties of metamagnetic $TbCo_{0.5}Mn_{0.5}O_{3.07}$ ceramics. *Journal of Materials Science* **49**, 3681–3686, https://doi.org/10.1007/s10853-014-8076-8 (2014).
18. Murthy, J. K. & Venimadhav, A. 4f-3d exchange coupling induced exchange bias and field induced Hopkinson peak effects in Gd_2CoMnO_6. *Journal of Alloys and Compounds* **719**, 341–346, https://doi.org/10.1016/j.jallcom.2017.05.203 (2017).
19. Liu, W. *et al*. Griffiths phase, spin-phonon coupling, and exchange bias effect in double perovskite Pr_2CoMnO_6. *Journal of Applied Physics* **116**, 193901, https://doi.org/10.1063/1.4902078 (2014).
20. Wang, X. L. *et al*. Structure and spin glass behaviour in non-metallic Yb_2CoMnO_6 perovskite manganite. *Journal of Magnetism and Magnetic Materials* **246**, 86–92, https://doi.org/10.1016/S0304-8853(02)00033-1 (2002).
21. Sazonov, A. P., Troyanchuk, I. O., Sikolenko, V. V., Szymczak, H. & Bärner, K. Effect of the oxygen nonstoichiometry on the structure and magnetic properties of $Nd_2CoMnO_{6+\delta}$ double perovskites. *physica status solidi (b)* **244**, 3367–3376, https://doi.org/10.1002/pssb.200642481 (2007).
22. Yáñez-Vilar, S. *et al*. Multiferroic behavior in the double-perovskite Lu_2MnCoO_6. *Physical Review B* **84**, 134427 (2011).
23. Choi, H., Moon, J., Kim, J., Choi, Y. & Lee, N. Single Crystal Growth of Multiferroic Double Perovskites: Yb_2CoMnO_6 and Lu_2CoMnO_6. *Crystals* **7**, 67 (2017).
24. Chikara, S. *et al*. Electric polarization observed in single crystals of multiferroic Lu_2MnCoO_6. *Physical Review B* **93**, 180405 (2016).
25. Kim, M. K. *et al*. Effects of different annealing atmospheres on magnetic properties in La_2CoMnO_6 single crystals. *Current Applied Physics* **15**, 776–779, https://doi.org/10.1016/j.cap.2015.04.009 (2015).
26. Lee, N. *et al*. Strong ferromagnetic-dielectric coupling in multiferroic Lu_2CoMnO_6 single crystals. *Applied Physics Letters* **104**, 112907, https://doi.org/10.1063/1.4869479 (2014).
27. Murthy, J. K., Chandrasekhar, K. D., Sudipta, M., Topwal, D. & Venimadhav, A. Giant magnetocaloric effect in Gd_2NiMnO_6 and Gd_2CoMnO_6 ferromagnetic insulators. *Journal of Physics D: Applied Physics* **48**, 355001 (2015).
28. Marsh, A. & Clark, C. C. Metamagnetism in the perovskite compound Gd_2CoMnO_6. *Philosophical Magazine* **19**, 449–463, https://doi.org/10.1080/14786436908216304 (1969).
29. Balli, M., Jandl, S., Fournier, P. & Gospodinov, M. M. Anisotropy-enhanced giant reversible rotating magnetocaloric effect in $HoMn_2O_5$ single crystals. *Applied Physics Letters* **104**, 232402, https://doi.org/10.1063/1.4880818 (2014).
30. Zhang, H. *et al*. Giant rotating magnetocaloric effect induced by highly texturing in polycrystalline DyNiSi compound. **5**, 11929, https://doi.org/10.1038/srep11929, https://www.nature.com/articles/srep11929#supplementary-information (2015).

Acknowledgements

This work was supported by the NRF Grant (NRF-2014S1A2A2028481, NRF-2015R1C1A1A02037744, NRF-2016R1C1B2013709, NRF-2017K2A9A2A08000278, and 2017R1A5A1014862 (SRC program: vdWMRC center)) and partially by the Yonsei University Future-leading Research Initiative of 2014 (2016-22-0099). J.Y.M. acknowledges the tuition support from the Hyundai Motor Chung Mong-Koo Foundation.

Author Contributions

Y.J.C. and N.L. designed the experiments. J.Y.M. and M.K.K. carried out the growth of single crystals and performed magnetic and heat capacity measurements. J.Y.M., Y.J.C., and N.L. analysed the data and prepared the manuscript. All authors have read and approved the final version of the manuscript.

Additional Information

Competing Interests: The authors declare that they have no competing interests.

Publisher's note: Springer Nature remains neutral with regard to jurisdictional claims in published maps and institutional affiliations.